blood®
Regular Article

HEMATOPOIESIS AND STEM CELLS

p57Kip2 regulates embryonic blood stem cells by controlling sympathoadrenal progenitor expansion

Chrysa Kapeni,[1] Leslie Nitsche,[1] Alastair M. Kilpatrick,[1] Nicola K. Wilson,[2] Kankan Xia,[2] Bahar Mirshekar-Syahkal,[2] Vashe Chandrakanthan,[3] Camille Malouf,[1] John E. Pimanda,[3,4] Berthold Göttgens,[2] Kristina Kirschner,[5,6] Simon R. Tomlinson,[1] and Katrin Ottersbach[1]

[1]Centre for Regenerative Medicine, Institute for Regeneration and Repair, University of Edinburgh, Edinburgh, United Kingdom; [2]Department of Haematology, Wellcome Trust-Medical Research Council Cambridge Stem Cell Institute, University of Cambridge, Cambridge, United Kingdom; [3]School of Medical Sciences, Lowy Cancer Research Centre, UNSW, Sydney, NSW, Australia; [4]Department of Haematology, The Prince of Wales Hospital, Sydney, NSW, Australia; [5]Institute of Cancer Sciences and [6]CRUK Beatson Institute for Cancer Research, University of Glasgow, Glasgow, United Kingdom

KEY POINTS

- p57Kip2 controls the size of the developing SNS by regulating sympathoadrenal progenitor proliferation.
- p57Kip2 regulates emerging blood stem cell numbers through noradrenaline production and β_2-adrenergic signaling.

Hematopoietic stem cells (HSCs) are of major clinical importance, and finding methods for their in vitro generation is a prime research focus. We show here that the cell cycle inhibitor p57Kip2/Cdkn1c limits the number of emerging HSCs by restricting the size of the sympathetic nervous system (SNS) and the amount of HSC-supportive catecholamines secreted by these cells. This regulation occurs at the SNS progenitor level and is in contrast to the cell-intrinsic function of p57Kip2 in maintaining adult HSCs, highlighting profound differences in cell cycle requirements of adult HSCs compared with their embryonic counterparts. Furthermore, this effect is specific to the aorta-gonad-mesonephros (AGM) region and shows that the AGM is the main contributor to early fetal liver colonization, as early fetal liver HSC numbers are equally affected. Using a range of antagonists in vivo, we show a requirement for intact β_2-adrenergic signaling for SNS-dependent HSC expansion. To gain further molecular insights, we have generated a single-cell RNA-sequencing data set of all Ngfr$^+$ sympathoadrenal cells around the dorsal aorta to dissect their differentiation pathway. Importantly, this not only defined the relevant p57Kip2-expressing SNS progenitor stage but also revealed that some neural crest cells, upon arrival at the aorta, are able to take an alternative differentiation pathway, giving rise to a subset of ventrally restricted mesenchymal cells that express important HSC-supportive factors. Neural crest cells thus appear to contribute to the AGM HSC niche via 2 different mechanisms: SNS-mediated catecholamine secretion and HSC-supportive mesenchymal cell production.

Introduction

Adult-repopulating hematopoietic stem cells (HSCs) are first detected at embryonic day 10.5 (E10.5) in the aorta-gonad-mesonephros (AGM) region of the mouse embryo.[1,2] They are derived from hemogenic endothelial cells (HECs) that can transdifferentiate into blood cells via a process termed endothelial-to-hematopoietic transition, as recently reviewed.[3-6] Although this process is believed to occur in several embryonic tissues harboring major vasculature, such as the head, yolk sac, placenta, vitelline, and umbilical arteries, it is the AGM region in which HSCs are first detected in robust numbers and where blood formation from the endothelium has been observed via live imaging.[7-10] This suggests that the AGM has a unique environment particularly suited for promoting HSC formation, which is supported by its remarkable ability to expand HSCs and their precursors in aggregate cultures.[11]

Relatively little is currently known about the AGM hematopoietic niche, specifically, the cell types and signals that regulate HSC generation, maintenance, and egress.[12] Cells with characteristics of mesenchymal stromal cells (MSCs) have been detected in the AGM, but their precise location and secretome remain unknown.[13] Tissues on the ventral side of the dorsal aorta are known to provide HSC regulatory signals belonging to the Notch, Hedgehog, and Bmp pathways.[14-20] HSC-supportive cytokines such as Scf and Thpo have also been detected in the subaortic mesenchyme.[19,21] In addition, our group previously reported that cells of the sympathetic nervous system (SNS), which develops in the vicinity of the aorta at the time of HSC generation, promote HSC production through the secretion of catecholamines, under the control of hematopoietic transcription factor Gata3.[22]

Here, we report that the cell cycle regulator p57Kip2 (Cdkn1c) controls the size of the sympathoadrenal (SA) compartment and thus the amount of catecholamines produced in the AGM, which has a direct influence on HSC numbers. We had previously shown that deletion of p57Kip2 leads to an increase in

HSCs at E12.5,[23] which is in stark contrast to the essential role of p57Kip2 in adult HSC maintenance and quiescence[24] and fetal liver (FL) HSC self-renewal.[25] We now provide further evidence that, unlike in adult HSC regulation, the effect of p57Kip2 on AGM HSCs occurs by regulating the proliferation of SA progenitors. We also further define the interaction between the developing hematopoietic and SNS and have generated a detailed characterization of the emerging SA compartment via single-cell RNA-sequencing (scRNA-Seq).

Methods

Mice and tissue preparations

Animal studies were performed following United Kingdom Home Office regulations. All animals were housed according to institutional guidelines, and experiments complied with the animal welfare laws. Details of tissue preparations from p57Kip2-null embryos,[26] Wnt1-Cre,[27] DsRed reporter,[28] and tdTomato[29] reporter embryos are provided in the supplemental Methods (available on the *Blood* Web site).

Transplantation experiments

Transplantations were performed as described previously.[23] Further details are provided in the supplemental Methods.

Adrenergic blocker administration in vivo

Each adrenergic receptor was blocked from E8 of gestation, as described in the supplemental Methods.

Catecholamine detection by high-performance liquid chromatography

High-performance liquid chromatography was performed in the Psychology Analytical Laboratory (Psychology Department, University of Cambridge). Details of the methods are provided in the supplemental Methods.

Flow cytometry and cell sorting

The staining in all the experiments was performed on ice in the dark for 30 minutes with antibodies as listed in the supplemental Methods.

Immunohistochemistry

Immunohistochemistry was performed as described previously.[23] Antibody details are provided in the supplemental Methods.

In situ hybridization

In situ hybridization was performed as described previously.[23] Probe details are provided in the supplemental Methods.

Gene expression analysis by real-time polymerase chain reaction

Real-time polymerase chain reaction (PCR) was performed with the Sybr Green method with primers listed in the supplemental Methods.

Single-cell RNA-sequencing

Detailed analysis methods are provided in the supplemental Methods. The Smart-seq2 protocol was used[30]; reads were aligned by using Kallisto (Linux v0.43.0[31]) and mapped to Mus_musculus.GRCm38.cdna.all.fa downloaded from Ensembl (www.ensembl.org) February 2017. Read quality was assessed by using FastQC and MultiQC,[32] and transcripts trimmed with Cutadapt.[33] Data were preprocessed following the single-cell transcriptomics workflow of Lun et al[34] and imported into R using the scater Bioconductor package (scater_1.18.6[35]) function readKallistoResults. We used the computeSumFactors function in the scran R package[34] to normalize within each plate and then scale plate samples to each other and the Cyclone prediction method[36] to assign cells into cell cycle phases, with the effect removed using limma (version 3.46.0[37]). The t-distributed stochastic neighbor embedding (t-SNE)[38] technique was used for dimensionality reduction. The edgeR Bioconductor package (version 3.32.1)[39] was used to identify significantly differentially expressed genes between cell clusters and the Slingshot Bioconductor package (version 1.8.0)[40] for cell lineage inference analysis. We used the GSEAPreranked tool (Gene Set Enrichment Analysis 4.1.0, build 27)[41] for gene set enrichment analysis and the liana package[42] to detect receptor-ligand interactions, for which identifiers were converted from murine to human using the biomaRt package (version 2.50.3.)[43] and soluble ligands selected with the OmnipathR package (version 3.3.20).[44]

Data accessibility

The scRNA-seq data from this study have been deposited in the Gene Expression Omnibus database[45] (accession number GSE139052).

Results

p57Kip2 deletion expands HSC numbers in the AGM and the early FL

We had previously reported an increase in repopulation activity of E12 p57Kip2-null AGMs and had suggested that this may be due to a migration defect in HSCs from the AGM to the FL.[23] In further transplantations, we have now also detected a trend toward higher HSC numbers in the E11 p57Kip2-null AGM (Figure 1A), albeit not as marked as at E12 (Figure 1B). Furthermore, significantly expanded HSC numbers were observed in the early FL (Figure 1C), which argues against a migration defect and instead suggests that the expansion of AGM HSCs translates into higher numbers colonizing the FL. This initial difference disappears over time as HSC numbers in the FL rapidly increase from E12 (Figure 1D). Interestingly, p57Kip2 deletion had no effect on HSC numbers in the E11 and E12 placenta and yolk sac (Figure 1E-H), despite high expression in the placenta (Figure 1I). This finding indicates that p57Kip2 is involved in HSC production specifically in the AGM, likely via regulating the number of preexisting HSCs as we noticed a slight decrease in quiescent hematopoietic cells in its absence (Figure 1J).

p57Kip2 is highly expressed in the SNS

Immunohistochemistry revealed weak p57Kip2 staining in individual $CD34^+$ endothelial cells (Figure 2A) and slightly stronger staining in subendothelial mesenchymal cells (Figure 2A-B). The most intense staining was observed in $Ngfr^+$ SA cells. For more quantitative data, these different $p57Kip2^+$ populations were sorted for real-time PCR analysis (Figure 2D; supplemental Figure 1), using CD34 as a marker for endothelial cells, Ngfr for SA cells, and Pdgfrß for mesenchymal cells, excluding SA cells (Figure 2C). Because p57Kip2 expression was reported in adult HSCs,[24,46-50] we also sorted $CD45^+CD34^+$ hematopoietic stem

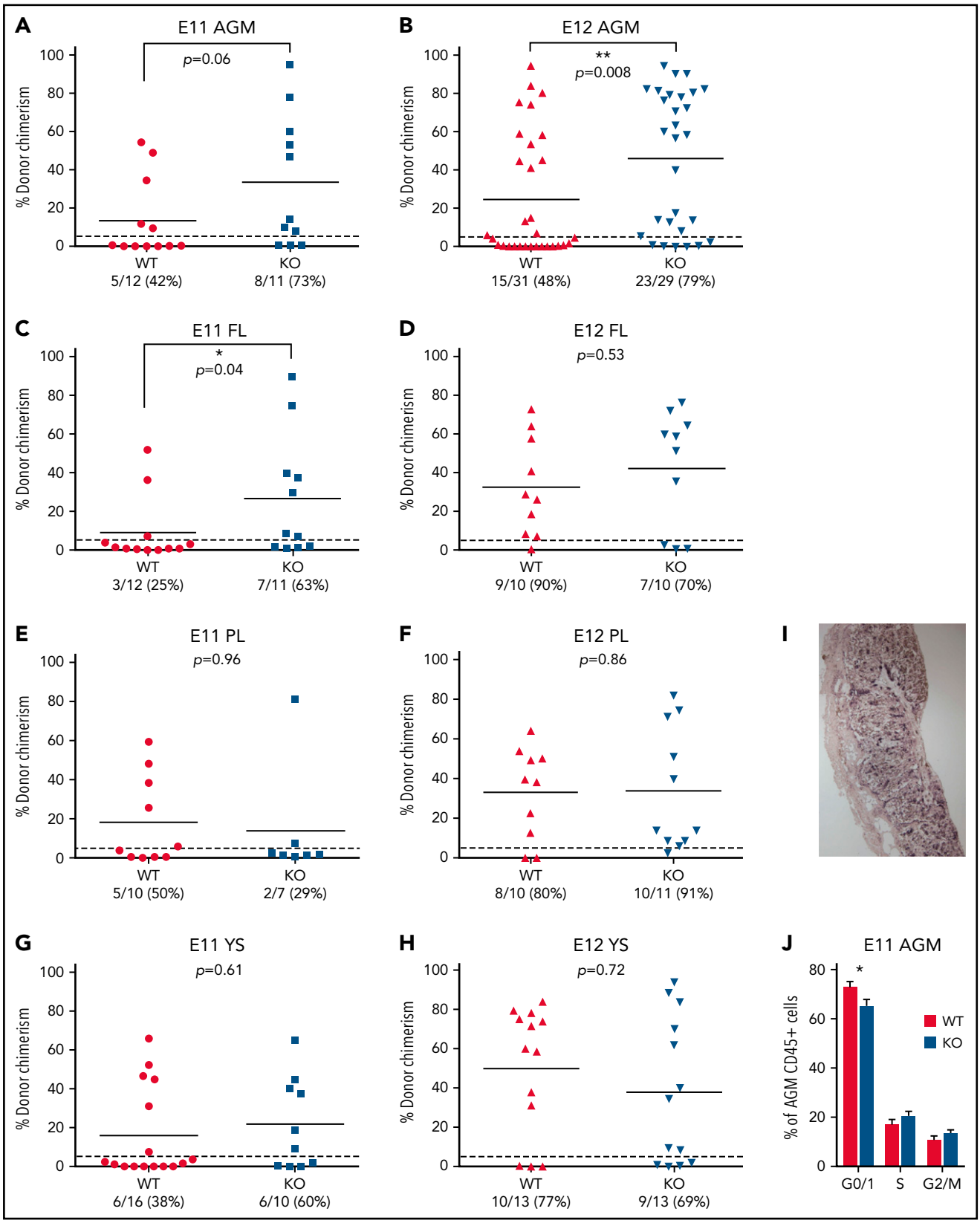

Figure 1. p57Kip2 deletion expands HSC numbers in the AGM and the early FL. Single-cell preparations of E11 AGM (0.5-1 embryo equivalent [ee]) (A), E12 AGM (1ee) (B), E11 FL (1ee) (C), E12 FL (0.05ee) (D), E11 placenta (PL, 2ee) (E), E12 PL (1ee) (F), E11 yolk sac (YS, 2ee) (G), and E12 YS (1ee) (H) from wild-type (WT) and p57Kip2-null (knockout [KO]) embryos were transplanted into irradiated recipients and donor chimerism determined after 4 months by flow cytometry. Data points represent individual recipients with the number of repopulated (>5% chimerism as indicated by the dashed line) recipients/total recipients indicated underneath each graph together with the percentage of repopulated mice. Solid line represents mean. (I) In situ hybridization with a *p57Kip2* RNA probe on transverse cryosections of E11 placenta showing high expression of *p57Kip2* in trophoblast cells of the placental labyrinth. (J) Percentage of $CD45^+$ hematopoietic cells from E11 p57Kip2 WT and KO embryos in the different cell cycle stages. 4′,6-Diamidino-2-phenylindole (DAPI)–stained $CD45^+$ E11 AGM cells were analyzed by flow cytometry. $^*P < .05$, $^{**}P < .01$, Mann-Whitney *U* test.

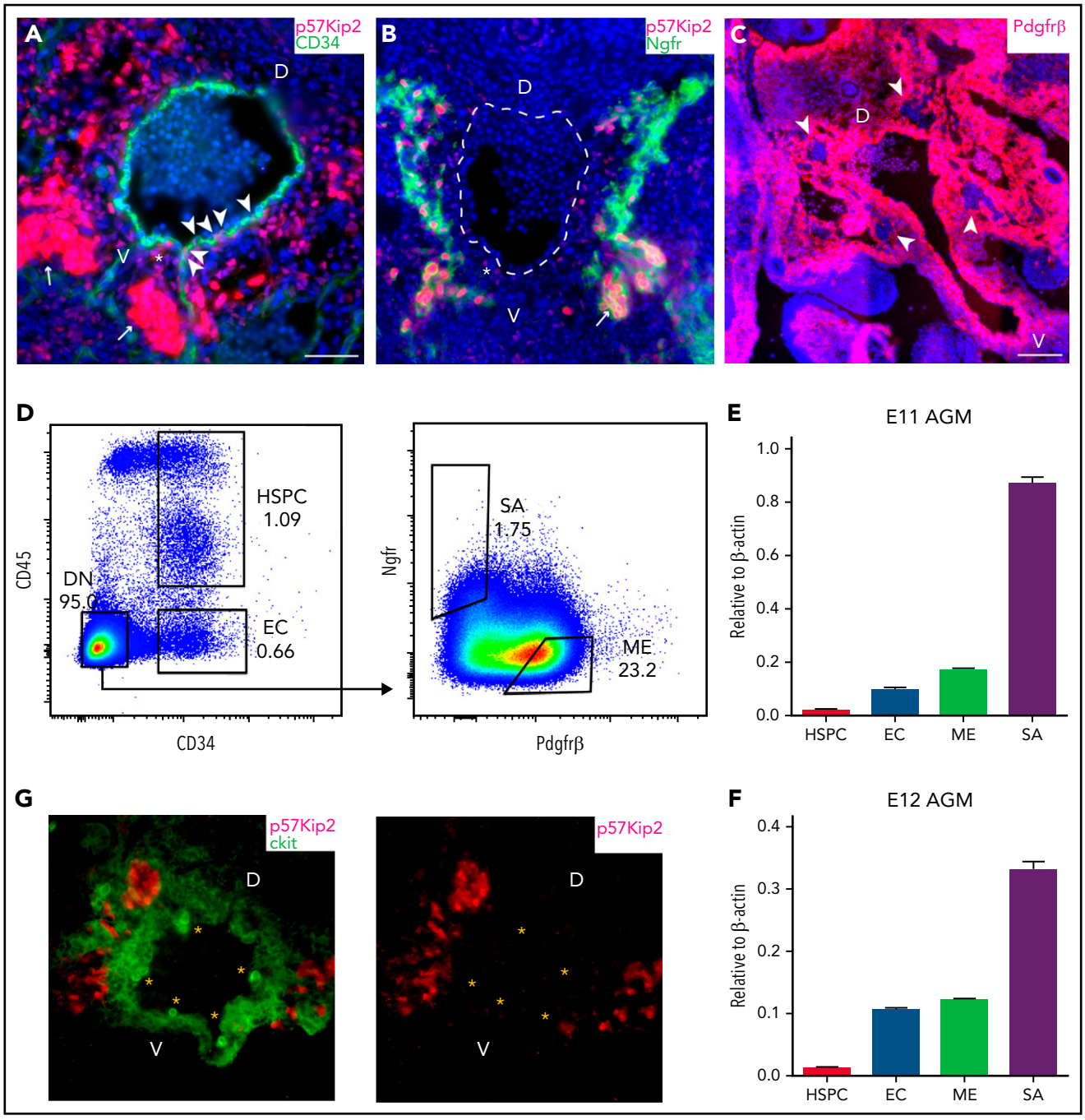

Figure 2. p57Kip2 is highly expressed in the SNS. Immunohistochemistry on cryosections from E11 wild-type embryos. (A) Immunostaining for p57Kip2 (red) and CD34 (green) with 4′,6-diamidino-2-phenylindole (DAPI) nuclear stain (blue). P57Kip2 expression is highlighted in endothelial cells (arrowheads), sub-endothelial mesenchyme (asterisk), and SA cells (arrows). (B) Immunostaining for p57Kip2 (red) and Ngfr (green) with DAPI nuclear stain (blue). P57Kip2 expression is highlighted in sub-endothelial mesenchyme (asterisk) and SA cells (arrows). Dashed line shows outline of the aorta. (C) Immunostaining for Pdgfrβ (red) with DAPI nuclear stain (blue). Exclusion of Pdgfrβ expression from SA cells is highlighted (arrows). Scale bars indicate 50 μm. (D) Sorting strategy for AGM subpopulations; HSPCs, $CD34^+CD45^+$; endothelial cells (EC), $CD34^+CD45^-$; SA cells, $Ngfr^+Pdgfr\beta^-$; mesenchymal cells (ME), Ngfr-Pdgfrβ+. Gating was based on fluorescence minus one controls as shown in supplemental Figure 1. (E, F) *p57Kip2* mRNA expression (relative to β-actin) by quantitative PCR in subpopulations sorted from E11 and E12 AGMs. n ≥ 3. Histogram represents mean ± SEM. (G) Immunostaining for p57Kip2 (red) and ckit (green) with DAPI nuclear stain (blue) on cryosections from E11 wild-type embryos. Intra-aortic clusters are highlighted by asterisks. D, dorsal; V, ventral.

and progenitor cells (HSPCs). The pattern did not change significantly between E11 and E12 and confirmed the strongest *p57Kip2* expression in SA cells and reduced levels in endothelial and mesenchymal cells (Figure 2E-F). Considering the reported function of p57Kip2 in adult HSCs, it was surprising that there was very little expression in AGM HSPCs. Immunohistochemistry confirmed the absence of p57Kip2 in emerging HSPCs in $ckit^+$ intra-aortic clusters (Figure 2G). This confirms our previous findings that embryonic HSCs have different properties from adult HSCs, including regulation of the cell cycle.[21,22]

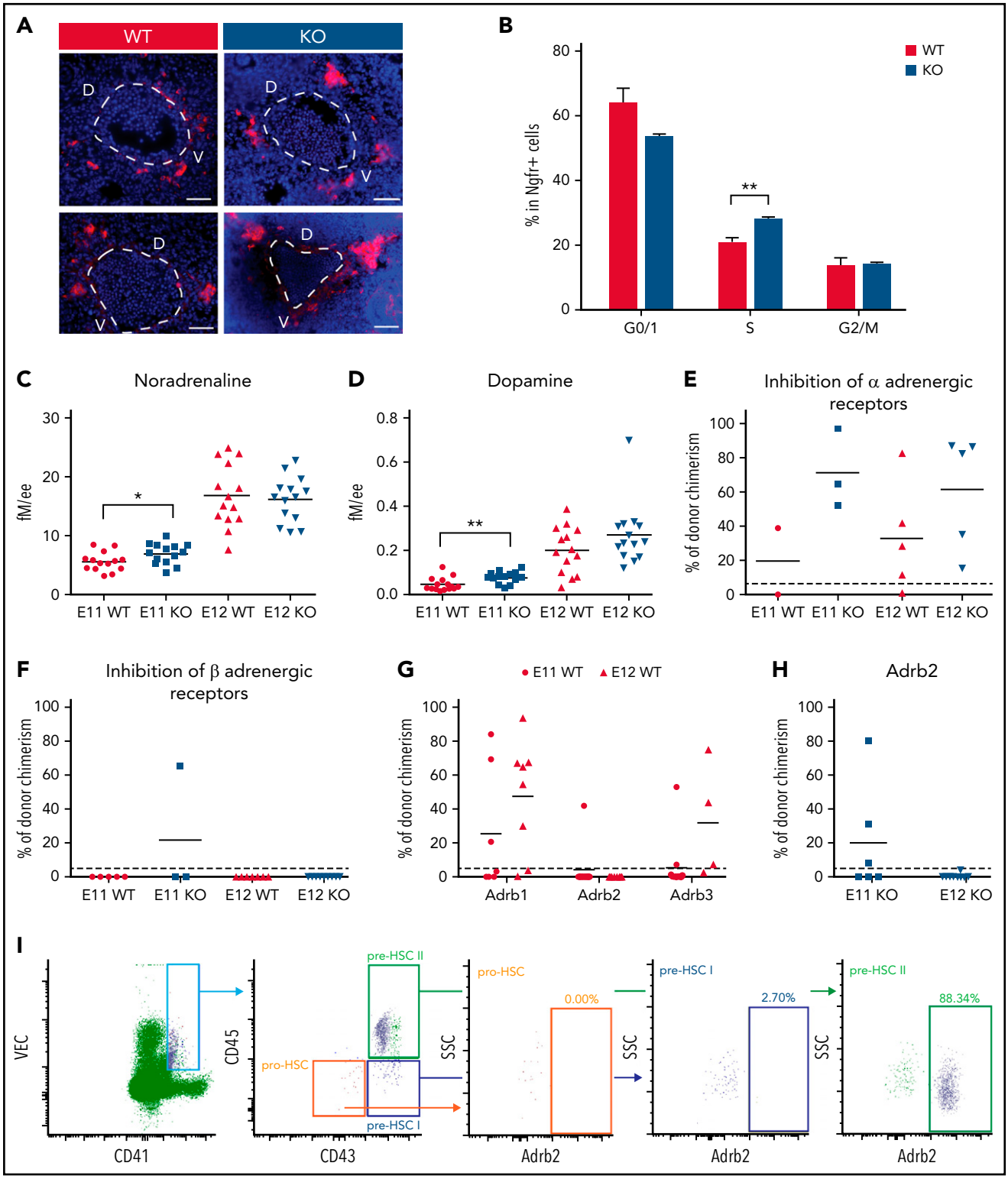

Figure 3. p57Kip2 increases HSC numbers through an expansion of the catecholamine-secreting SA compartment. (A) Immunostaining for Th (red) with 4′,6-diamidino-2-phenylindole (DAPI) nuclear stain (blue) on cryosections from E11 p57Kip2 wild-type (WT) and knockout (KO) embryos. Dashed line shows outline of the aorta. Scale bars indicate 50 μm. (B) Percentage of Ngfr$^+$ SA cells from E11 p57Kip2 WT and KO embryos in the different cell cycle stages. DAPI–stained Ngfr$^+$ E11 AGM cells were analyzed by flow cytometry. Quantification of the catecholamines noradrenaline (C) and dopamine (D) by high-performance liquid chromatography in individual p57Kip2 WT and KO E11 and E12 AGMs. Concentration is measured in femtomole per embryo equivalent (fM/ee). Black lines denote the mean; n = 14. Donor chimerism in recipients of AGM cells from E11 or E12 p57Kip2 WT or KO embryos treated in utero with the α-adrenergic receptor (Adra1 and Adra2) blocker phentolamine (E) or the β-adrenergic receptor blocker propranolol (F). (G) Donor chimerism in recipients of AGM cells from E11 or E12 p57Kip2 WT embryos treated in utero with the specific β-adrenergic receptor blockers betaxolol (for Adrb1), ICI 118 551 (for Adrb2), and SR 59230A (for Adrb3). (H) Donor chimerism in recipients of AGM cells from E11 or E12 p57Kip2 KO embryos treated in utero with the Adrb2 blocker ICI 118 551. Data points represent chimerism in individual recipients of 1ee (1-3 separate experiments for each condition) determined by flow cytometry after 4 months, with the dashed line indicating 5% threshold and the solid line the mean. (I) Flow cytometry analysis of Adrb2 expression on pro-HSCs (VEC$^+$CD41$^+$CD43$^-$CD45$^-$), pre-HSC I (VEC$^+$CD41$^+$CD43$^+$CD45$^-$), and pre-HSC II (VEC$^+$CD41$^+$CD43$^+$CD45$^+$) from E10.5 AGMs. *$P < .05$, **$P < .01$, two-tailed, unpaired t test. D, dorsal; SSC, side scatter; V, ventral; VEC, VE-Cadherin.

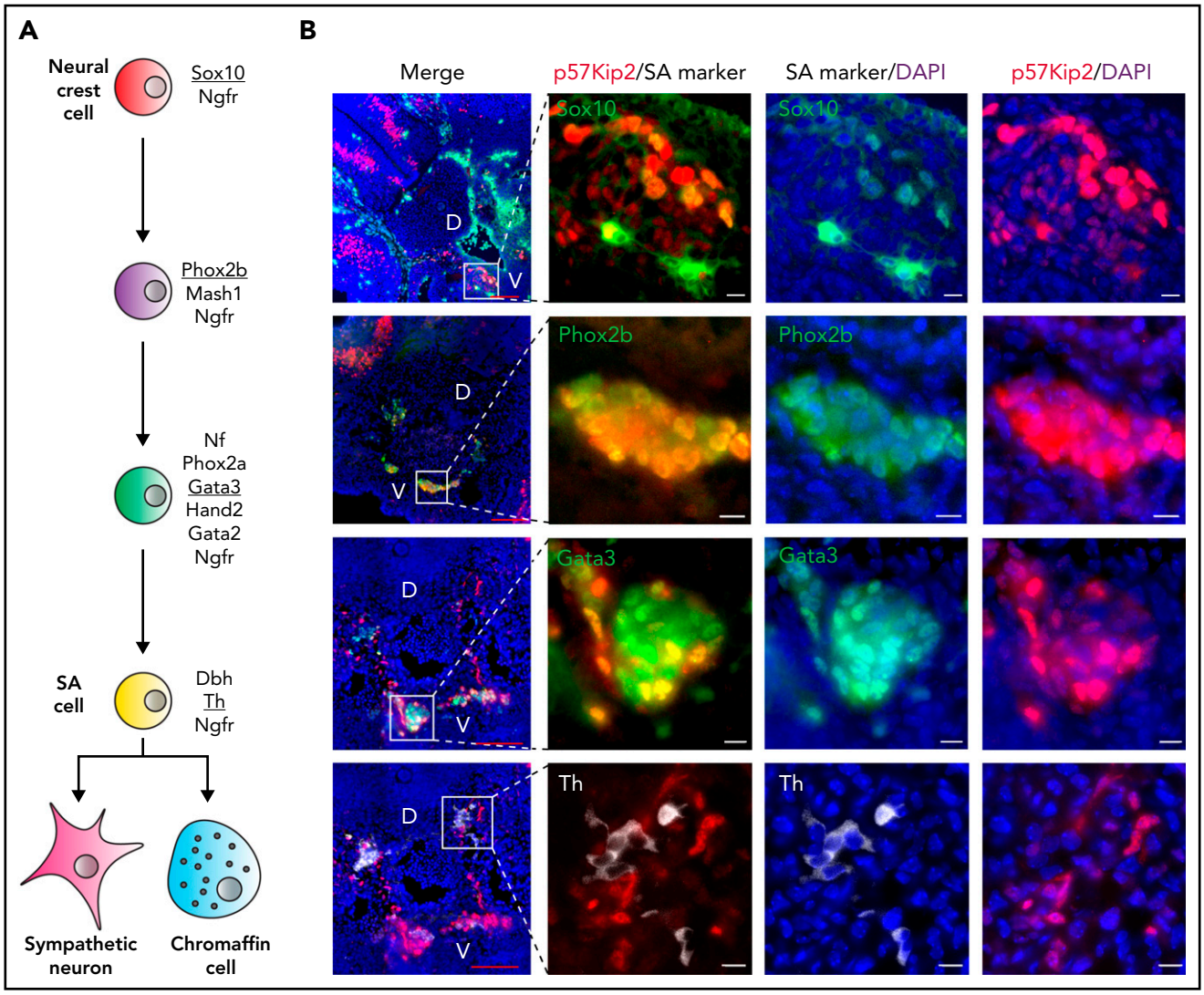

Figure 4. p57Kip2 is expressed in SA progenitor cells. (A) Schematic depiction of maturation stages in the SA lineage as defined by listed marker expression. Underlined markers were used in immunohistochemistry in panel B. (B) Immunohistochemical staining of E11 wild-type embryo cryosections for p57Kip2 (red), Sox (green), Phox2b (green), Gata3 (green) and Th (white), with 4′,6-diamidino-2-phenylindole (DAPI) as nuclear counterstain (blue). Close-ups of boxed areas in merged images are shown. White scale bars equal 10 μm and red bars equal 100 μm. D, dorsal; V, ventral.

p57Kip2 regulates the size of the catecholamine-secreting SA compartment

Considering the strong p57Kip2 expression in the SNS and the role of SA cells in promoting HSC production via catecholamines, we analyzed the effect of p57Kip2 deletion on SNS development. Immunohistochemical staining for the SA marker tyrosine hydroxylase (Th), the enzyme for catecholamine synthesis, revealed an expansion of the SA compartment (Figure 3A), as confirmed by using real-time PCR (supplemental Figure 2A) and intracellular flow cytometry staining for Gata3 and Th (supplemental Figure 2B-C), although the latter did not reach significance. HSPC, endothelial, and mesenchymal populations were not expanded (supplemental Figure 2D-F). Because p57Kip2 is a cell cycle inhibitor, the expansion of the SA compartment occurred via enhanced proliferation, with a higher percentage of $Ngfr^{+}$ cells in S phase in the absence of p57Kip2 (Figure 3B). Interestingly, of all the embryonic tissues harboring HSCs, only the AGM expressed robust levels of *Th* (supplemental Figure 2G-H), suggesting that the functional interaction between the developing hematopoietic and SNS is AGM specific.

To establish whether SNS expansion translates into higher production of catecholamines, we measured catecholamine levels by using high-performance liquid chromatography. A pilot experiment revealed that noradrenaline is the most abundant catecholamine in the AGM, with much higher concentration there than in other hematopoietic tissues (supplemental Figure 2I). Noradrenaline levels at E11 were significantly higher in the p57Kip2-null AGMs; however, this normalized at E12 (Figure 3C). Levels of dopamine, a noradrenaline precursor, were also significantly higher in E11 p57Kip2KO AGMs, with a similar trend at E12 (Figure 3D).

Catecholamines exert their effects by binding to adrenergic receptors, of which there are 2 families, α and β. Blocking α-adrenergic receptors had no effect on HSC numbers in wild-type AGMs and did not abrogate the HSC expansion

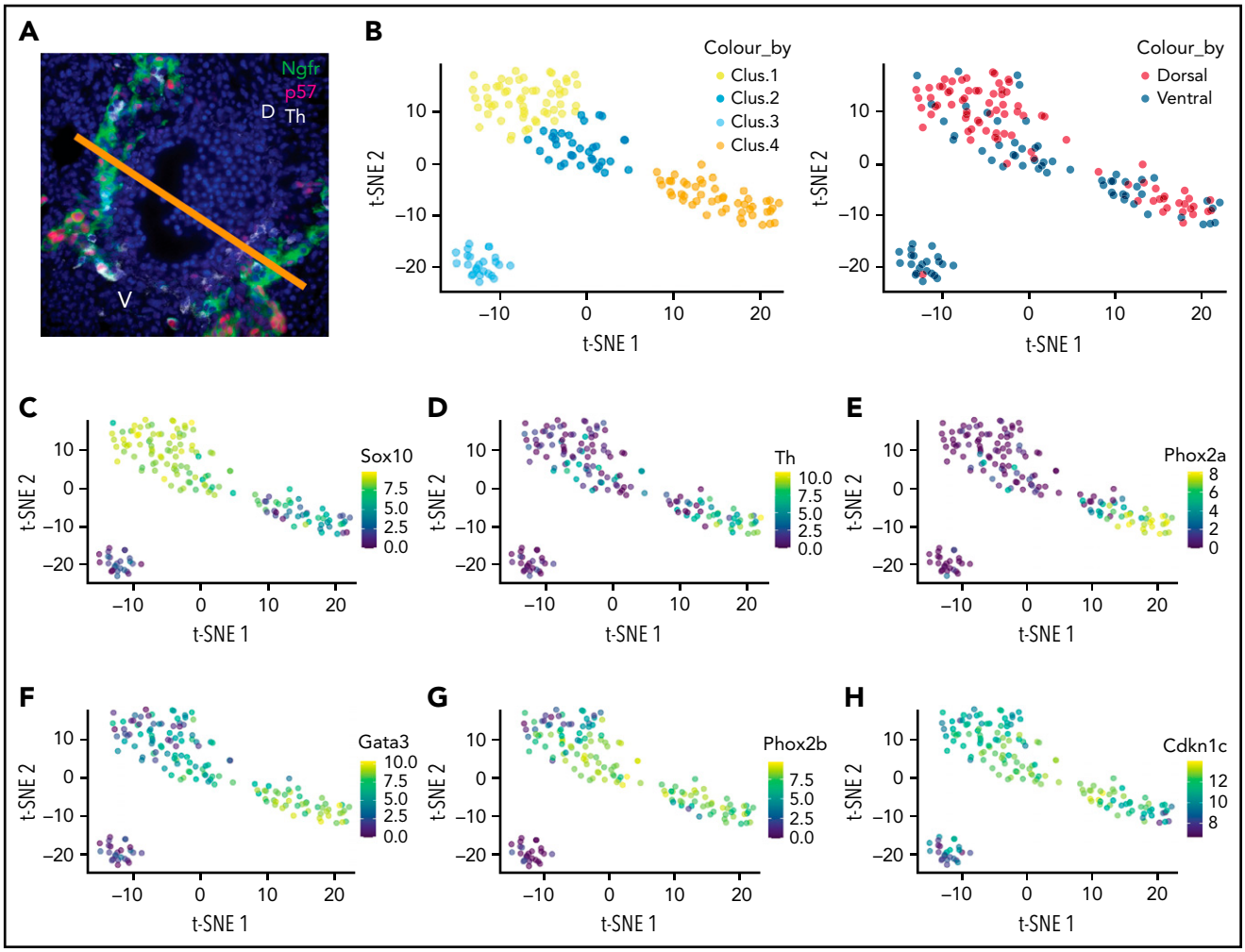

Figure 5. scRNA-Seq reveals neural crest differentiation pathways. (A) Immunohistochemical staining of E11 wild-type embryo cryosection for Ngfr (green), p57Kip2 (red), and Th (white). Bar represents ventral (V) vs dorsal (D) subdissection. (B) t-SNE plot of remaining 4 clusters after cell cycle correction (left) and colored according to ventral and dorsal origin (right). t-SNE gene expression plots colored for expression levels of SNS genes *Sox10* (C), *Th* (D), *Phox2a* (E), *Gata3* (F), *Phox2b* (G) and *Cdkn1c/p57Kip2* (H).

observed in p57Kip2KO AGMs (Figure 3E). In contrast, blocking β-adrenergic receptors had a profound negative impact on HSC activity (Figure 3F). Because there are three β-adrenergic receptors, we used more specific antagonists, which revealed that Adrb2 is required for HSC production in wild-type AGMs (Figure 3G), which is also the case in p57Kip2-null AGMs (Figure 3H). We have previously shown that a subset of E11.5 $CD34^+$ and $CD45^+$ AGM cells express Adrb2 on their surface.[22] To further map the emergence of catecholamine-responding cells, we concentrated on HSC emergence at E10.5, which has been further sub-dissected into pro-HSCs, pre-HSC I, and pre-HSC II via the sequential expression of CD41, CD43, and CD45.[51] Interestingly, there was little to no expression of Adrb2 at the early stages of HSC maturation (pro-HSCs and pre-HSC I), with a remarkable upregulation of Adrb2 on pre-HSC II (Figure 3I).

p57Kip2 is expressed in SA progenitor cells

To better define the cell type in which p57Kip2 is expressed, we performed immunohistochemistry with established markers of SA differentiation, as reviewed elsewhere[52] (Figure 4A). The SA lineage derives from $Sox10^+$ neural crest cells, which migrate from the neural tube to the aorta at around E10. Upon arrival, their commitment to the SA fate is initiated by upregulation of the master regulator Phox2b. Further maturation involves upregulation of Gata3, which is required for the expression of Th, allowing these cells to become catecholamine-producing cells of the adrenal anlage (ventrally) or the sympathetic ganglia (dorsally).

We detected little overlap between p57Kip2 and Sox10, whereas overlap with Phox2b was complete (Figure 4B). p57Kip2 expression then becomes more restricted, only partially overlapping with Gata3, and displaying an almost mutually exclusive pattern with Th. These results suggest that p57Kip2 expression initiates with the commitment of neural crest cells to the SA lineage but being gradually downregulated as these cells fully mature.

scRNA-Seq reveals neural crest differentiation pathways

scRNA-Seq was performed to better define the differentiation pathway. Because cell surface expression of Ngfr captures all SA

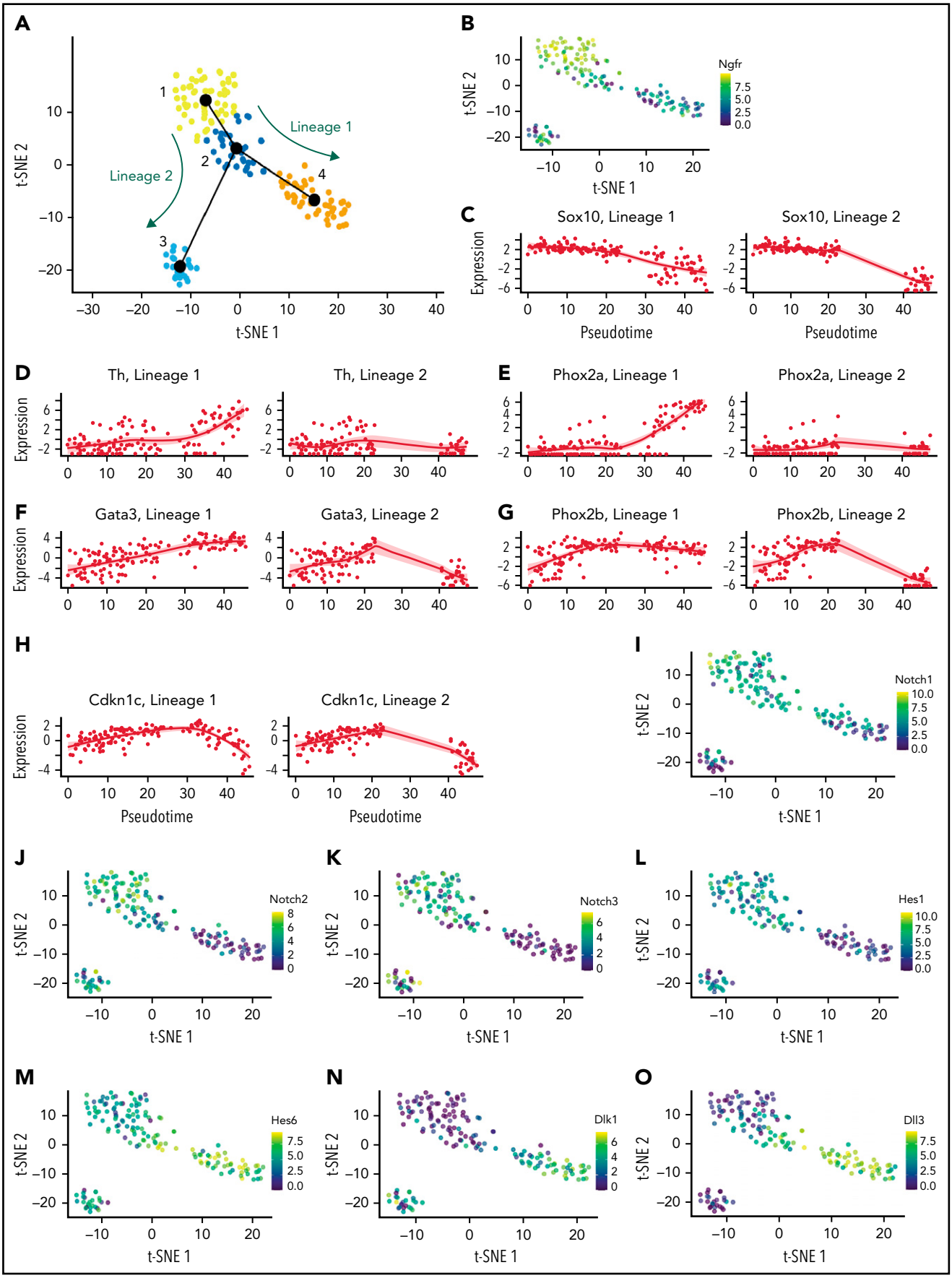

Figure 6.

cells (Figure 5A), this marker was used to sort single cells from E11 AGMs, excluding mesenchymal cells (Ngfr$^+$ Pdgfrß$^-$). HSCs are preferentially located on the ventral side of the aorta.[53] To detect factors in the ventral SA domain that may contribute to the polarized localization of HSCs, dissected aortae with the surrounding mesenchyme were first cut along the longitudinal axis to separate the ventral from the dorsal side before cell sorting. Cell clustering and dimensionality reduction using t-SNE identified 6 clusters (supplemental Figure 3A). After removing a cluster that appeared to be composed of contaminating macrophages (Cluster 4) (supplemental Figure 3B-J) and cell cycle correction, resulting in the fusion of clusters 1 and 2 (supplemental Figure 3K), the remaining cells were grouped into 4 clusters (Figure 5B). Differential expression analysis was performed to determine the 40 most differentially expressed genes for each cluster (supplemental Figure 4).

To assign the clusters to stages of SA differentiation, we investigated the expression of stage-specific markers (Figure 4A). *Sox10* expression was highest in cluster 1 (Figure 5C), suggesting that this cluster is enriched for neural crest cells, whereas *Th* expression, the end point of SA differentiation, is mostly confined to cluster 4 (Figure 5D). The late SA marker *Phox2a* is also upregulated in cluster 4 (Figure 5E), whereas *Gata3* expression initiates already in cluster 2 (Figure 5F). As suggested from immunohistochemistry (Figure 4), *Phox2b* and *p57Kip2* display a similar expression pattern. They are both upregulated in some cluster 1 cells, followed by the highest expression in cluster 2 and, at least for *p57Kip2*, downregulation in cluster 4 (Figure 5G-H). Cluster 1 and cluster 4 thus appear to mark the 2 end points of SA differentiation, with cluster 2 being an intermediate stage.

Notch signaling is downregulated upon SA maturation

To further confirm this potential differentiation pathway, we performed cell lineage inference with Slingshot, a method that is designed for modeling developmental trajectories in single-cell transcriptomic data and allows for integration of known developmental stages. Because the SA lineage derives from Sox10$^+$ neural crest cells, we defined the cluster with the highest *Sox10* expression (Figure 5C) as a starting point. Lineage inference analysis revealed that neural crest cells from cluster 1 can take 2 alternative differentiation pathways, ending in clusters 3 (Lineage 2) or 4 (Lineage 1), via an intermediate population (cluster 2), in which divergence of the 2 fates initiates (Figure 6A). *Ngfr*-expressing cells were found in all clusters, although expression was highest in the neural crest cluster (Figure 6B). *Sox10* expression is downregulated along the trajectories, which occurs more gradually toward cluster 4 and more rapidly toward cluster 3 (Figure 6C). The trajectory toward cluster 4 is the classic SA differentiation pathway marked by a sharp upregulation of *Th* (Figure 6D). *Phox2a* is similarly upregulated in cluster 4 (Figure 6E), whereas *Gata3* expression, albeit highest in cluster 4, initiates noticeably earlier (Figure 6F). *Gata3* expression is dependent on Phox2b,[54] the expression of which is clearly initiated before *Gata3* (Figure 6G). Expression of *p57Kip2*/*Cdkn1c* is highest in the intermediate cluster 2, going into cluster 4 (Figures 6H and 5H), likely making this the stage at which SA progenitors are expanded in *p57Kip2*-null embryos.

We noticed differential expression of members of the Notch pathway among the clusters (Figure 6I-O). Expression of the 3 receptors, *Notch1-3*, was highest at the neural crest stage, and all 3 were downregulated by the final stage of SA differentiation in cluster 4 (Figure 6I-K). One of the main mediators of Notch activation is Hes1, which displayed an expression pattern similar to that of *Notch1-3* (Figure 6L). Another member of this family, Hes6, however, displayed the opposite pattern, with upregulation coincident with SA differentiation (Figure 6M). Interestingly, Hes6 was reportedly not activated by Notch but instead served as an inhibitor of Hes1, thereby promoting neural differentiation.[55] Two Notch ligands, Dll3 and Dlk1, also displayed upregulation along the SA differentiation pathway (Figure 6N-O), and we have previously shown that *Dlk1* expression in the SNS is Gata3 dependent.[18] As with Hes6, Dll3 and Dlk1 are known antagonists of Notch signaling.[56-59] Taken together, this suggests that Notch activity maintains neural crest identity and needs to be attenuated for these cells to commit to a SA fate, which may be achieved through the upregulation of Notch signaling inhibitors such as Hes6, Dll3, and Dlk1. In support of this action, it was shown in chick embryos that expression of the constitutively active intracellular Notch domain inhibited sympathetic neuron differentiation from neural crest progenitors, while inhibition of Notch signaling increased neuron numbers.[60]

Neural crest cells can take an alternative differentiation path toward a mesenchymal fate in the AGM

Our lineage inference analysis (Figure 6A) suggests that neural crest cells can differentiate along 2 alternative pathways. Differentiation into cluster 4 cells represents the well-described SA differentiation path as marked by upregulation of key markers such as *Tubb3* and *Dbh* (supplemental Figure 5A). Interestingly, differentiation along the alternative pathway toward cluster 3 is spatially restricted to the ventral side of the aorta (Figure 5B). The region underneath the ventral endothelium contains a heterogeneous population of mesenchymal cells, many of which secrete factors supporting AGM hematopoiesis, as reviewed elsewhere.[12] Furthermore, the existence of cells with properties of MSCs in the AGM has been reported.[13] In that context, it is interesting that neuroepithelial cells were shown to give rise to a transient wave of MSCs via a neural crest intermediate.[61] We therefore hypothesized that a subset of neural crest cells upon arrival receives local signals that induce them to differentiate along the mesenchymal lineage instead of the SA lineage. Indeed, a subset of cluster 3 cells expresses mesenchymal markers such as *Bmper* and *Pdgfra* (Figure 7A-B).[17] To determine how similar the cluster 3 cells are to subaortic mesenchymal cells, we integrated a scRNA-Seq data set from Pdgfrβ$^+$ Ngfr$^-$ mesenchymal cells isolated from the ventral halves of E11 AGMs. Putative Ngfr$^+$ mesenchymal cells clustered more closely

Figure 6. Notch signaling is downregulated upon SA maturation. (A) t-SNE plot of 4 clusters with slingshot-identified lineage trajectory nodes superimposed. (B) t-SNE gene expression plot colored for expression levels of *Ngfr*. Pseudotime plots for SNS differentiation markers *Sox10* (C), *Th* (D), *Phox2a* (E), *Gata3* (F), *Phox2b* (G) and *Cdkn1c/p57Kip2* (H). t-SNE gene expression plots colored for expression levels of Notch pathway-associated genes *Notch1* (I), *Notch2* (J), *Notch3* (K), *Hes1* (L), *Hes6* (M), *Dlk1* (N) and *Dll3* (O).

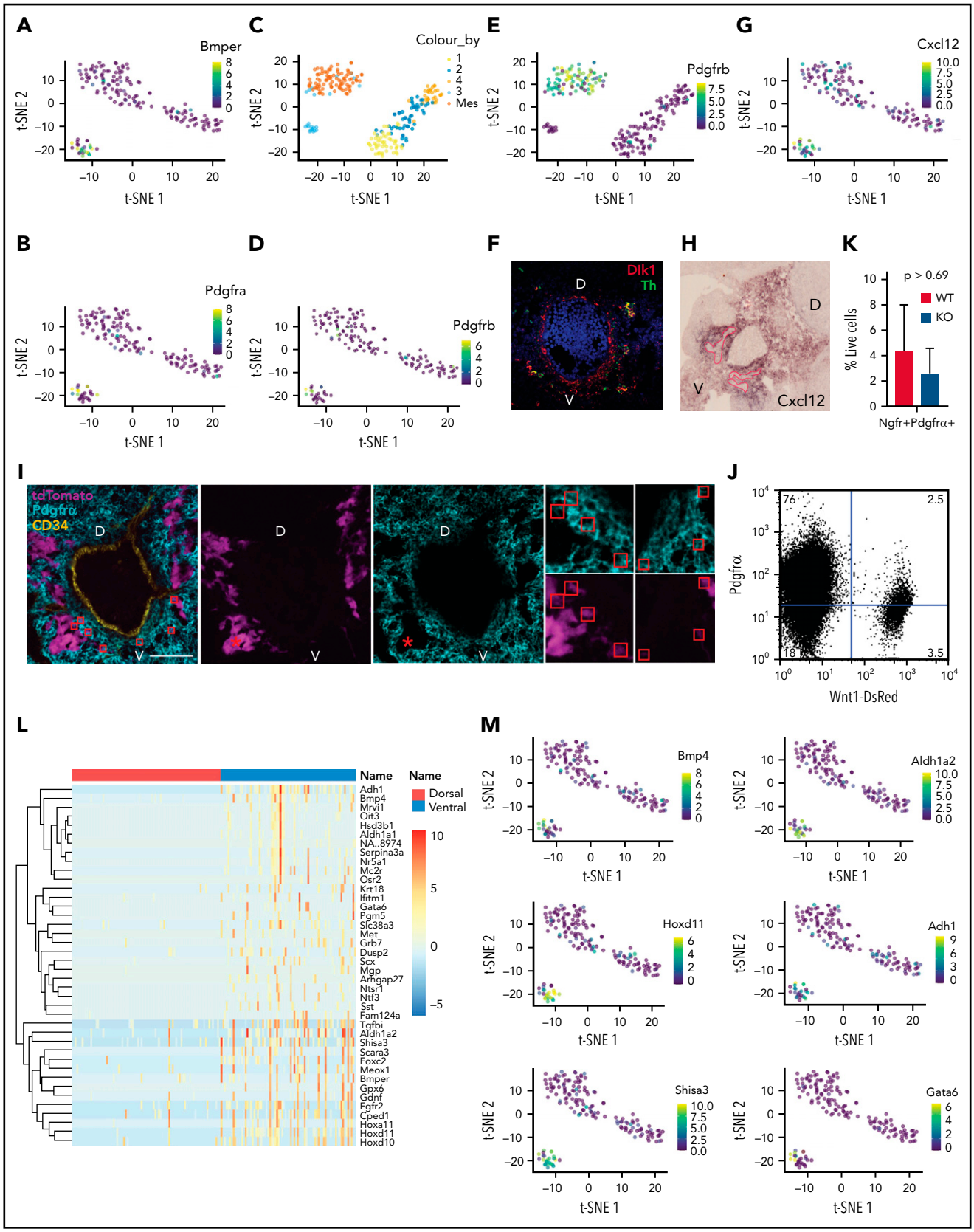

Figure 7.

with the Pdgfrβ$^+$ Ngfr$^-$ subaortic mesenchymal cells, with some cells even integrating into the bigger Pdgfrβ$^+$ Ngfr$^-$ mesenchymal cluster when projected into a shared t-SNE space (Figure 7C). Even though cluster 3 cells were sorted as Pdgfrβ$^-$ Ngfr$^+$, a subpopulation of these already upregulate *Pdgfrb* (Figure 7D), which largely overlaps with the cells that also express *Pdgfra* (Figure 7B) and the majority of which cluster with the larger Pdgfrβ$^+$ Ngfr$^-$ mesenchymal cluster (Figure 7E). Differential expression analysis of cluster 3 cells compared with all other cells was subjected to Gene Set Enrichment Analysis. This further supported the putative mesenchymal character of cluster 3, as significantly enriched Gene Ontology terms included "Heart development" and "Signaling pathways downstream of Tgfb." To locate cluster 3 cells within the AGM, we conducted immunostaining for Dlk1, which was upregulated in cells of both cluster 3 and cluster 4 (Figure 6N). Coexpression with Th identified cluster 4 cells in ventrolateral and dorsolateral patches, whereas Dlk1$^+$ Th$^-$ cells were concentrated in the ventral mesenchyme (Figure 7F).

Bmper was recently identified as a regulator for AGM HSC maturation.[17] We therefore checked for the presence of other important HSC niche factors and detected *Cxcl12* expression in the majority of cluster 3 cells (Figure 7G). In situ hybridization confirmed strong expression of *Cxcl12* in the ventral mesenchyme, while being excluded from the SA domain (Figure 7H). In addition, Gene Ontology terms such as "Cytokine-cytokine receptor interaction" and "Chemokines bind chemokine receptors" were enriched. To explore this potential niche function further, we searched for ligand-receptor pairs between cluster 3 cells and AGM HSCs, using a published AGM HSC scRNA-Seq data set.[62] Among the soluble ligands expressed by cluster 3 cells were indeed a number of cytokines, including *Angpt2*, *Fgf10*, *Il4*, and *Tnf* (supplemental Figure 6A). Of interest may also be *Calr*, as it has been linked to myeloproliferative neoplasms but never before to AGM hematopoiesis.[63,64] We performed the same analysis for SNS clusters 1, 2 and 4, which also detected *Calr*, *Fgf10*, *Il4*, and *Tnf* (supplemental Figure 6B).

To provide functional evidence that neural crest cells can give rise to mesenchymal cells, we performed lineage tracing experiments by crossing Wnt1-Cre mice, which mark neural crest cells and their progeny,[27] with a reporter line. Although the neural crest cells predominantly gave rise to SNS cells that do not express the mesenchymal marker Pdgfrα (Figure 7I), we detected a few double-positive cells on the ventral side. Flow cytometry confirmed that a substantial percentage of AGM Pdgfrα$^+$ mesenchymal cells in the AGM are indeed derived from neural crest cells (Figure 7J). This Ngfr$^+$ Pdgfrα$^+$ population was not expanded in p57Kip2-null AGMs (Figure 7K).

The detection of HSC regulators prompted us to mine our data set for other polarized factors, differentially expressed between ventrally and dorsally derived Ngfr$^+$ cells. Among the genes upregulated in the ventral cells were known HSC regulators such as *Mgp*,[65] *Ntf3*,[66] and *Tgfbi*,[67] some of which have been shown to be expressed in the ventral mesenchyme, such as *Bmper*[17] and *Bmp4*[16,19] (Figure 7L). The expression of the majority of the ventrally upregulated genes was restricted to cluster 3 (Figure 7M), showing that they are the strongest contributor to the polarized expression of genes within the Ngfr$^+$ populations and may represent an important subset of HSC niche cells. The hematopoietic support function of the ventrally derived cells is further supported by Gene Ontology terms such as "Peptide ligand-binding receptors," "Factors involved in megakaryocyte development and platelet production," "Systemic lupus erythematosus," and "Retinol metabolism." Interestingly, although some genes such as *Bmper*, *Cxcl12*, and *Shisa3* are widely expressed in cluster 3 (Figure 7A,G,M), others such as *Bmp4* and *Hoxd11* displayed almost mutually exclusive expression, with *Bmp4* expression overlapping with that of *Pdgfra* and *Pdgfrb* (Figure 7B,D,M). This suggests that subpopulations within cluster 3 may have different developmental origins. Indeed, some of the cells in cluster 3 express *Meox1* (supplemental Figure 5B), indicating that these may be of somitic mesodermal origin.[68]

Overall, our results suggest that neural crest cells not only regulate HSC development in the aorta via the secretion of catecholamines from SA cells but may also contribute a population of mesenchymal cells to the HSC niche that secrete HSC-supportive factors.

Discussion

We report here that p57Kip2 restricts AGM HSC numbers through regulation of the size of the SA pool and therefore catecholamine levels. This is in stark contrast to the essential cell-intrinsic role of p57Kip2 in maintaining adult HSC functionality.[24,25] In fact, we show that p57Kip2 expression in AGM HSPCs is almost absent. This is another example of how embryonic HSCs differ from their adult counterparts in the way they regulate their cell cycle,[22] respond to DNA damage-inducing agents[21] and are affected by mutations linked to hematologic malignancies.[21,69] These differences are clearly important to regenerative medicine and human disease. The reason why the HSC expansion phenotype does not change to the exhaustion phenotype reported for adult HSCs[24] 4 months post-transplant is explained by our previous observation that embryonic HSCs do not fully convert to adult HSCs in the bone marrow, suggesting that they require migration via the FL to complete their maturation.[21] Although our experiments with blockers of β-adrenergic signaling clearly show the importance of catecholamines in HSC production in the AGM, the levels of which are regulated by p57Kip2, we cannot rule out that the deletion of p57Kip2 has an additional

Figure 7. Neural crest cells can take an alternative differentiation path toward a mesenchymal fate upon arrival at the aorta. t-SNE plots colored for the expression levels of mesenchymal genes *Bmper* (A) and *Pdgfra* (B). (C) t-SNE plot of Ngfr$^+$ cells with Pdgfrβ$^+$Ngfr$^-$ mesenchymal cells sorted from the ventral E11 AGM. t-SNE plots of Ngfr$^+$ cells (D) and Ngfr$^+$ cells with Pdgfrβ$^+$Ngfr$^-$ mesenchymal cells (E) colored for the expression levels of *Pdgfrb*. (F) Immunohistochemical staining of E11 wild-type embryo cryosection for Dlk1 (red), Th (green), and DAPI (blue). (G) t-SNE gene expression plot colored for the expression of *Cxcl12*. (H) In situ hybridization staining on E11 wild-type AGM cryosection with a RNA probe for *Cxcl12*. Red lines outline ventral (V) *Cxcl12*-negative SNS patches. (I) Immunohistochemistry of E11.5 Wnt1-Cre$^+$ tdTomato$^+$ embryo with CD34 staining in yellow, tdTomato in magenta, and Pdgfrα in cyan. Asterisk denotes tdTomato$^+$Pdgfrα$^-$ SNS compartment; red boxes highlight tdTomato$^+$Pdgfrα$^+$ cells. Scale bar equals 100 μm. (J) Flow cytometry analysis of E11 Wnt1-Cre$^+$ DsRed$^+$ CD31$^-$ AGM cells costained with an antibody to Pdgfrα. (K) Quantification of Ngfr$^+$ Pdgfrα$^+$ cells detected by flow cytometry analysis of E11 wild-type (WT) and p57Kip2 knockout (KO) AGM cells. A *t*-test was performed; error bars = SEM; n = 3. (L) Heatmap of the top 40 ventrally expressed genes in Ngfr$^+$ cells. (M) t-SNE gene expression plots colored for the expression of genes upregulated in ventrally derived Ngfr1$^+$ cells. D, dorsal; V, ventral.

effect on HEC numbers, as we detected p57Kip2 expression in a subset of endothelial cells (ECs). The role of cell cycle regulation during the endothelial-to-hematopoietic transition (EHT) has not been fully defined. Data suggest that ECs and HECs are largely quiescent but that re-entry into the cell cycle occurs toward the end of EHT, with proliferation of HSPCs occurring in intra-aortic clusters.[70-74] Whether p57Kip2 is indeed expressed in HECs and controls some of these cell cycle changes during EHT, and whether these cell cycle changes are essential for the completion of the EHT, will have to be addressed in the future.

The current study also delivers further insights into the way in which the definitive hematopoietic system and the SNS interact during their formation. Their interaction in the adult bone marrow has been well studied, with data supporting a direct effect of catecholamines via Adrb2 on the surface of HSPCs[75] or via an indirect mechanism mediated by Adrb3 on stromal cells.[76] Our results with adrenergic receptor-specific inhibitors and Adrb2 expression on emerging HSCs[22] suggest that the effect of catecholamines (predominantly noradrenaline) is likely to be direct in the AGM. In line with previous findings from adult HSCs,[75] our data also suggest that catecholamines promote the proliferation of pre-existing HSCs. Interestingly, this interplay seems to be restricted to the AGM region, which is the main catecholamine producer at this point in development. The fact that HSC expansion in p57Kip2-null AGMs translates into higher numbers of HSCs in the early FL suggests that the AGM is the main contributor to FL seeding at this stage.

The single-cell transcriptome analysis of $Ngfr^{+}$ cells in the AGM region has provided novel insights into the differentiation pathways that neural crest cells undertake after reaching the dorsal aorta. It appears that downregulation of Notch signaling in SA progenitors is required for terminal differentiation. Interestingly, this is also the case for the completion of hematopoietic specification from HECs in the AGM,[77-79] although the mechanisms may differ. Upregulation of Jag was shown to restrict Notch activity in hematopoietic specification, while we observed an upregulation of the inhibitors Dlk1, Dll3, and Hes6.

Intriguingly, our cell lineage inference analysis highlighted a branching point in neural crest cell differentiation, with one path leading to SA differentiation, while an alternative pathway results in the generation of cells with a mesenchymal character. There have been several reports of trunk neural crest cells differentiating into mesenchymal cells. An early study suggested that trunk neural crest cells produce the first, yet transient, wave of MSCs,[61] while subsequent studies provide evidence that at least a subset of bone marrow MSCs, with HSC niche activities (eg, through the secretion of Cxcl12), are derived from trunk neural crest cells,[80,81] which may migrate to the bone marrow via the AGM.[82] Furthermore, a more recent study in zebrafish embryos reported Pdgf signaling-mediated migration of neural crest cells to the dorsal aorta where they promote HSC specification through direct interaction with HECs and provision of signals that are catecholamine independent.[83] Interestingly, we have also detected upregulation of Pdgf signaling in cluster 3 cells, and they were shown to express HSC regulators such as *Cxcl12* and *Bmp4*. Whether these cells are indeed involved in AGM hematopoiesis and might even interact directly with HECs remains to be shown. Cxcl12 and Bmp4 also regulate the migration of neural crest cells and SA progenitors toward the dorsal aorta (as reviewed elsewhere[84]), while Cxcl12 and Scf guide primordial germ cell migration through the AGM region.[85] It may thus be an exciting possibility that cluster 3 cells are part of a signaling center that coordinates the migration/regulation of several important cell types (HSCs, neural crest, and primordial germ cells) simultaneously.

Acknowledgments

The authors are indebted to the staff of the animal facilities, both at the Cambridge Institute for Medical Research and the Centre for Regenerative Medicine, for their support with animal experiments. They are also grateful to the flow cytometry teams at both of these institutes, Reiner Schulte, Chiara Cossetti, and Michal Maj in Cambridge and Fiona Rossi and Claire Cryer in Edinburgh, for excellent cell-sorting services and help with flow cytometry analyses. The authors are also very grateful to Dr Jean-François Brunet for providing the Phox2b antibody.

Core facilities at the Edinburgh Centre for Regenerative Medicine were supported by centre grant MR/K017047/1. This work was funded by the National Health and Medical Research Council of Australia (1102589, J.E.P.; 1061593, V.C.), a Bloodwise Bennett Senior Fellowship (10015, K.O.), and the Kay Kendall Leukaemia Fund (K.O.). This research was also funded in part by the Wellcome Trust and the UKRI Medical Research Council.

Authorship

Contribution: C.K. performed and designed the majority of experiments and wrote the manuscript; L.N., A.M.K., and K.K. performed bioinformatics analyses; N.K.W. and B.G. provided advice and assistance with scRNA-Seq experiment; L.N., V.C., K.X., B.M.-S., and C.M. performed experiments; J.E.P. provided essential data; S.R.T. designed, performed, and supervised the bioinformatics analysis of the scRNA-Seq data; and K.O. conceived and supervised the study and wrote the manuscript.

Conflict-of-interest disclosure: The authors declare no competing financial interests.

ORCID profiles: C.K., 0000-0003-0408-2106; L.N., 0000-0002-0312-7467; A.M.K., 0000-0002-4795-8799; N.K.W., 0000-0003-0865-7333; B.M.-S., 0000-0002-2337-9442; V.C., 0000-0002-4314-5029; K.K., 0000-0001-7607-8670; S.R.T., 0000-0003-3465-9156; K.O., 0000-0002-6880-4895.

Correspondence: Katrin Ottersbach, Centre for Regenerative Medicine, Institute for Regeneration and Repair, Edinburgh BioQuarter, 5 Little France Dr, University of Edinburgh, Edinburgh EH16 4UU; e-mail: katrin.ottersbach@ed.ac.uk.

Footnotes

Submitted 15 November 2021; accepted 13 May 2022; prepublished online on *Blood* First Edition 2 June 2022. DOI 10.1182/blood.2021014853.

The scRNA-seq data from this study have been deposited in the Gene Expression Omnibus database[46] (accession number GSE139052).

The online version of this article contains a data supplement.

There is a *Blood* Commentary on this article in this issue.

The publication costs of this article were defrayed in part by page charge payment. Therefore, and solely to indicate this fact, this article is hereby marked "advertisement" in accordance with 18 USC section 1734.

REFERENCES

1. Medvinsky A, Dzierzak E. Definitive hematopoiesis is autonomously initiated by the AGM region. *Cell*. 1996;86(6):897-906.
2. Müller AM, Medvinsky A, Strouboulis J, Grosveld F, Dzierzak E. Development of hematopoietic stem cell activity in the mouse embryo. *Immunity*. 1994;1(4):291-301.
3. Ciau-Uitz A, Monteiro R, Kirmizitas A, Patient R. Developmental hematopoiesis: ontogeny, genetic programming and conservation. *Exp Hematol*. 2014;42(8):669-683.
4. Dzierzak E, de Pater E. Regulation of blood stem cell development. *Curr Top Dev Biol*. 2016;118:1-20.
5. Lacaud G, Kouskoff V. Hemangioblast, hemogenic endothelium, and primitive versus definitive hematopoiesis. *Exp Hematol*. 2017;49:19-24.
6. Ottersbach K. Endothelial-to-haematopoietic transition: an update on the process of making blood. *Biochem Soc Trans*. 2019;47(2):591-601.
7. Boisset JC, van Cappellen W, Andrieu-Soler C, Galjart N, Dzierzak E, Robin C. In vivo imaging of haematopoietic cells emerging from the mouse aortic endothelium. *Nature*. 2010;464(7285):116-120.
8. Gordon-Keylock S, Sobiesiak M, Rybtsov S, Moore K, Medvinsky A. Mouse extraembryonic arterial vessels harbor precursors capable of maturing into definitive HSCs. *Blood*. 2013;122(14):2338-2345.
9. Li Z, Lan Y, He W, et al. Mouse embryonic head as a site for hematopoietic stem cell development. *Cell Stem Cell*. 2012;11(5):663-675.
10. Rhodes KE, Gekas C, Wang Y, et al. The emergence of hematopoietic stem cells is initiated in the placental vasculature in the absence of circulation. *Cell Stem Cell*. 2008;2(3):252-263.
11. Taoudi S, Gonneau C, Moore K, et al. Extensive hematopoietic stem cell generation in the AGM region via maturation of VE-cadherin+CD45+ pre-definitive HSCs. *Cell Stem Cell*. 2008;3(1):99-108.
12. Mirshekar-Syahkal B, Fitch SR, Ottersbach K. Concise review: from greenhouse to garden: the changing soil of the hematopoietic stem cell microenvironment during development. *Stem Cells*. 2014;32(7):1691-1700.
13. Mendes SC, Robin C, Dzierzak E. Mesenchymal progenitor cells localize within hematopoietic sites throughout ontogeny. *Development*. 2005;132(5):1127-1136.
14. Crisan M, Kartalaei PS, Vink CS, et al. BMP signalling differentially regulates distinct haematopoietic stem cell types [published correction appears in *Nat Commun*. 2015;6:8793]. *Nat Commun*. 2015;6(1):8040.
15. Crisan M, Solaimani Kartalaei P, Neagu A, et al. BMP and Hedgehog regulate distinct AGM hematopoietic stem cells ex vivo. *Stem Cell Reports*. 2016;6(3):383-395.
16. Durand C, Robin C, Bollerot K, Baron MH, Ottersbach K, Dzierzak E. Embryonic stromal clones reveal developmental regulators of definitive hematopoietic stem cells. *Proc Natl Acad Sci U S A*. 2007;104(52):20838-20843.
17. McGarvey AC, Rybtsov S, Souilhol C, et al. A molecular roadmap of the AGM region reveals BMPER as a novel regulator of HSC maturation. *J Exp Med*. 2017;214(12):3731-3751.
18. Mirshekar-Syahkal B, Haak E, Kimber GM, et al. Dlk1 is a negative regulator of emerging hematopoietic stem and progenitor cells. *Haematologica*. 2013;98(2):163-171.
19. Souilhol C, Gonneau C, Lendinez JG, et al. Inductive interactions mediated by interplay of asymmetric signalling underlie development of adult haematopoietic stem cells. *Nat Commun*. 2016;7(1):10784.
20. Yvernogeau L, Klaus A, Maas J, et al. Multispecies RNA tomography reveals regulators of hematopoietic stem cell birth in the embryonic aorta. *Blood*. 2020;136(7):831-844.
21. Mascarenhas MI, Bacon WA, Kapeni C, et al. Analysis of Jak2 signaling reveals resistance of mouse embryonic hematopoietic stem cells to myeloproliferative disease mutation. *Blood*. 2016;127(19):2298-2309.
22. Fitch SR, Kimber GM, Wilson NK, et al. Signaling from the sympathetic nervous system regulates hematopoietic stem cell emergence during embryogenesis. *Cell Stem Cell*. 2012;11(4):554-566.
23. Mascarenhas MI, Parker A, Dzierzak E, Ottersbach K. Identification of novel regulators of hematopoietic stem cell development through refinement of stem cell localization and expression profiling. *Blood*. 2009;114(21):4645-4653.
24. Matsumoto A, Takeishi S, Kanie T, et al. p57 is required for quiescence and maintenance of adult hematopoietic stem cells. *Cell Stem Cell*. 2011;9(3):262-271.
25. Zou P, Yoshihara H, Hosokawa K, et al. p57(Kip2) and p27(Kip1) cooperate to maintain hematopoietic stem cell quiescence through interactions with Hsc70. *Cell Stem Cell*. 2011;9(3):247-261.
26. Zhang P, Liégeois NJ, Wong C, et al. Altered cell differentiation and proliferation in mice lacking p57KIP2 indicates a role in Beckwith-Wiedemann syndrome. *Nature*. 1997;387(6629):151-158.
27. Lewis AE, Vasudevan HN, O'Neill AK, Soriano P, Bush JO. The widely used Wnt1-Cre transgene causes developmental phenotypes by ectopic activation of Wnt signaling. *Dev Biol*. 2013;379(2):229-234.
28. Vintersten K, Monetti C, Gertsenstein M, et al. Mouse in red: red fluorescent protein expression in mouse ES cells, embryos, and adult animals. *Genesis*. 2004;40(4):241-246.
29. Madisen L, Zwingman TA, Sunkin SM, et al. A robust and high-throughput Cre reporting and characterization system for the whole mouse brain. *Nat Neurosci*. 2010;13(1):133-140.
30. Picelli S, Faridani OR, Björklund AK, Winberg G, Sagasser S, Sandberg R. Full-length RNA-seq from single cells using Smart-seq2. *Nat Protoc*. 2014;9(1):171-181.
31. Bray NL, Pimentel H, Melsted P, Pachter L. Near-optimal probabilistic RNA-seq quantification [published correction appears in *Nat Biotechnol*. 2016;34(8):888]. *Nat Biotechnol*. 2016;34(5):525-527.
32. Ewels P, Magnusson M, Lundin S, Käller M. MultiQC: summarize analysis results for multiple tools and samples in a single report. *Bioinformatics*. 2016;32(19):3047-3048.
33. Martin M. Cutadapt removes adapter sequences from high-throughput sequencing reads. *EMBnet J*. 2011;17(1):10-12.
34. Lun AT, McCarthy DJ, Marioni JC. A step-by-step workflow for low-level analysis of single-cell RNA-seq data with Bioconductor. *F1000 Res*. 2016;5:2122.
35. McCarthy DJ, Campbell KR, Lun AT, Wills QF. Scater: pre-processing, quality control, normalization and visualization of single-cell RNA-seq data in R. *Bioinformatics*. 2017;33(8):1179-1186.
36. Scialdone A, Natarajan KN, Saraiva LR, et al. Computational assignment of cell-cycle stage from single-cell transcriptome data. *Methods*. 2015;85:54-61.
37. Ritchie ME, Phipson B, Wu D, et al. limma powers differential expression analyses for RNA-sequencing and microarray studies. *Nucleic Acids Res*. 2015;43(7):e47.
38. van der Maaten L, Hinton G. Visualizing data using t-SNE. *J Mach Learn Res*. 2008;9:2579-2605.
39. Robinson MD, McCarthy DJ, Smyth GK. edgeR: a bioconductor package for differential expression analysis of digital gene expression data. *Bioinformatics*. 2010;26(1):139-140.
40. Street K, Risso D, Fletcher RB, et al. Slingshot: cell lineage and pseudotime inference for single-cell transcriptomics. *BMC Genomics*. 2018;19(1):477.
41. Subramanian A, Tamayo P, Mootha VK, et al. Gene set enrichment analysis: a knowledge-based approach for interpreting genome-wide expression profiles. *Proc Natl Acad Sci U S A*. 2005;102(43):15545-15550.
42. Dimitrov D, Türei D, Garrido-Rodriguez M, et al. Comparison of methods and resources for cell-cell communication inference from single-cell RNA-Seq data. *Nat Commun*. 2022;13(1):3224.
43. Durinck S, Spellman PT, Birney E, Huber W. Mapping identifiers for the integration of genomic datasets with the R/Bioconductor package biomaRt. *Nat Protoc*. 2009;4(8):1184-1191.
44. Türei D, Valdeolivas A, Gul L, et al. Integrated intra- and intercellular signaling knowledge for multicellular omics analysis. *Mol Syst Biol*. 2021;17(3):e9923.
45. Edgar R, Domrachev M, Lash AE. Gene Expression Omnibus: NCBI gene expression

and hybridization array data repository. *Nucleic Acids Res.* 2002;30(1):207-210.

46. Miyamoto K, Araki KY, Naka K, et al. Foxo3a is essential for maintenance of the hematopoietic stem cell pool. *Cell Stem Cell.* 2007;1(1):101-112.

47. Passegué E, Wagers AJ, Giuriato S, Anderson WC, Weissman IL. Global analysis of proliferation and cell cycle gene expression in the regulation of hematopoietic stem and progenitor cell fates. *J Exp Med.* 2005;202(11):1599-1611.

48. Qian H, Georges-Labouesse E, Nyström A, et al. Distinct roles of integrins alpha6 and alpha4 in homing of fetal liver hematopoietic stem and progenitor cells. *Blood.* 2007;110(7): 2399-2407.

49. Wilson NK, Kent DG, Buettner F, et al. Combined single-cell functional and gene expression analysis resolves heterogeneity within stem cell populations. *Cell Stem Cell.* 2015;16(6):712-724.

50. Yamazaki S, Iwama A, Takayanagi S, et al. Cytokine signals modulated via lipid rafts mimic niche signals and induce hibernation in hematopoietic stem cells. *EMBO J.* 2006; 25(15):3515-3523.

51. Rybtsov S, Batsivari A, Bilotkach K, et al. Tracing the origin of the HSC hierarchy reveals an SCF-dependent, IL-3-independent CD43(-) embryonic precursor. *Stem Cell Reports.* 2014;3(3):489-501.

52. Huber K. The sympathoadrenal cell lineage: specification, diversification, and new perspectives. *Dev Biol.* 2006;298(2):335-343.

53. Taoudi S, Medvinsky A. Functional identification of the hematopoietic stem cell niche in the ventral domain of the embryonic dorsal aorta. *Proc Natl Acad Sci U S A.* 2007; 104(22):9399-9403.

54. Tsarovina K, Pattyn A, Stubbusch J, et al. Essential role of Gata transcription factors in sympathetic neuron development. *Development.* 2004;131(19):4775-4786.

55. Bae S, Bessho Y, Hojo M, Kageyama R. The bHLH gene Hes6, an inhibitor of Hes1, promotes neuronal differentiation. *Development.* 2000;127(13):2933-2943.

56. Baladrón V, Ruiz-Hidalgo MJ, Nueda ML, et al. dlk acts as a negative regulator of Notch1 activation through interactions with specific EGF-like repeats. *Exp Cell Res.* 2005;303(2):343-359.

57. Bray SJ, Takada S, Harrison E, Shen SC, Ferguson-Smith AC. The atypical mammalian ligand Delta-like homologue 1 (Dlk1) can regulate Notch signalling in Drosophila. *BMC Dev Biol.* 2008;8(1):11.

58. Ladi E, Nichols JT, Ge W, et al. The divergent DSL ligand Dll3 does not activate Notch signaling but cell autonomously attenuates signaling induced by other DSL ligands. *J Cell Biol.* 2005;170(6):983-992.

59. Nueda ML, Baladrón V, Sánchez-Solana B, Ballesteros MA, Laborda J. The EGF-like protein dlk1 inhibits notch signaling and potentiates adipogenesis of mesenchymal cells. *J Mol Biol.* 2007;367(5):1281-1293.

60. Tsarovina K, Schellenberger J, Schneider C, Rohrer H. Progenitor cell maintenance and neurogenesis in sympathetic ganglia involves Notch signaling. *Mol Cell Neurosci.* 2008;37(1):20-31.

61. Takashima Y, Era T, Nakao K, et al. Neuroepithelial cells supply an initial transient wave of MSC differentiation. *Cell.* 2007;129(7):1377-1388.

62. Vink CS, Calero-Nieto FJ, Wang X, et al. Iterative single-cell analyses define the transcriptome of the first functional hematopoietic stem cells. *Cell Rep.* 2020;31(6):107627.

63. Klampfl T, Gisslinger H, Harutyunyan AS, et al. Somatic mutations of calreticulin in myeloproliferative neoplasms. *N Engl J Med.* 2013;369(25):2379-2390.

64. Nangalia J, Massie CE, Baxter EJ, et al. Somatic CALR mutations in myeloproliferative neoplasms with nonmutated JAK2. *N Engl J Med.* 2013;369(25):2391-2405.

65. Kuronuma K, Yokoi A, Fukuoka T, et al. Matrix Gla protein maintains normal and malignant hematopoietic progenitor cells by interacting with bone morphogenetic protein-4. *Heliyon.* 2020;6(4):e03743.

66. Celebi B, Mantovani D, Pineault N. Insulin-like growth factor binding protein-2 and neurotrophin 3 synergize together to promote the expansion of hematopoietic cells ex vivo. *Cytokine.* 2012;58(3):327-331.

67. Klamer SE, Dorland YL, Kleijer M, et al. TGFBI expressed by bone marrow niche cells and hematopoietic stem and progenitor cells regulates hematopoiesis. *Stem Cells Dev.* 2018;27(21):1494-1506.

68. Mankoo BS, Skuntz S, Harrigan I, et al. The concerted action of Meox homeobox genes is required upstream of genetic pathways essential for the formation, patterning and differentiation of somites. *Development.* 2003;130(19):4655-4664.

69. Barrett NA, Malouf C, Kapeni C, et al. Mll-AF4 confers enhanced self-renewal and lymphoid potential during a restricted window in development. *Cell Rep.* 2016;16(4):1039-1054.

70. Batsivari A, Rybtsov S, Souilhol C, et al. Understanding hematopoietic stem cell development through functional correlation of their proliferative status with the intra-aortic cluster architecture. *Stem Cell Reports.* 2017;8(6):1549-1562.

71. Canu G, Athanasiadis E, Grandy RA, et al. Analysis of endothelial-to-haematopoietic transition at the single cell level identifies cell cycle regulation as a driver of differentiation. *Genome Biol.* 2020;21(1): 157.

72. Fadlullah MZH, Neo WH, Lie-A-Ling M, et al. Murine AGM single-cell profiling identifies a continuum of hemogenic endothelium differentiation marked by ACE. *Blood.* 2022;139(3): 343-356.

73. Oatley M, Bölükbası OV, Svensson V, et al. Single-cell transcriptomics identifies CD44 as a marker and regulator of endothelial to haematopoietic transition. *Nat Commun.* 2020;11(1):586.

74. Zeng Y, He J, Bai Z, et al. Tracing the first hematopoietic stem cell generation in human embryo by single-cell RNA sequencing. *Cell Res.* 2019;29(11):881-894.

75. Spiegel A, Shivtiel S, Kalinkovich A, et al. Catecholaminergic neurotransmitters regulate migration and repopulation of immature human CD34+ cells through Wnt signaling. *Nat Immunol.* 2007;8(10):1123-1131.

76. Méndez-Ferrer S, Lucas D, Battista M, Frenette PS. Haematopoietic stem cell release is regulated by circadian oscillations. *Nature.* 2008;452(7186):442-447.

77. Gama-Norton L, Ferrando E, Ruiz-Herguido C, et al. Notch signal strength controls cell fate in the haemogenic endothelium [published correction appears in *Nat Commun.* 2016;7:10978]. *Nat Commun.* 2015;6(1):8510.

78. Lizama CO, Hawkins JS, Schmitt CE, et al. Repression of arterial genes in hemogenic endothelium is sufficient for haematopoietic fate acquisition. *Nat Commun.* 2015;6(1): 7739.

79. Souilhol C, Lendinez JG, Rybtsov S, et al. Developing HSCs become Notch independent by the end of maturation in the AGM region. *Blood.* 2016;128(12):1567-1577.

80. Isern J, García-García A, Martín AM, et al. The neural crest is a source of mesenchymal stem cells with specialized hematopoietic stem cell niche function. *eLife.* 2014;3: e03696.

81. Morikawa S, Mabuchi Y, Niibe K, et al. Development of mesenchymal stem cells partially originate from the neural crest. *Biochem Biophys Res Commun.* 2009;379(4): 1114-1119.

82. Nagoshi N, Shibata S, Kubota Y, et al. Ontogeny and multipotency of neural crest-derived stem cells in mouse bone marrow, dorsal root ganglia, and whisker pad. *Cell Stem Cell.* 2008;2(4):392-403.

83. Damm EW, Clements WK. Pdgf signalling guides neural crest contribution to the haematopoietic stem cell specification niche. *Nat Cell Biol.* 2017;19(5):457-467.

84. Saito D, Takahashi Y. Sympatho-adrenal morphogenesis regulated by the dorsal aorta. *Mech Dev.* 2015;138(pt 1):2-7.

85. Chen SR, Zheng QS, Zhang Y, Gao F, Liu YX. Disruption of genital ridge development causes aberrant primordial germ cell proliferation but does not affect their directional migration. *BMC Biol.* 2013;11(1):22.